Phenyl(carbonyl)bis(trimethylphosphine)iridium(I). To $[IrCl(CO)(PMe_3)_2]$ (**1a**, 629 mg, 1.54 mmol) in C_6H_6 (30 mL) was added PhLi (0.93 mL of a 2 M solution in 70:30 v/v cyclohexane/ether, 1.85 mmol), and the mixture was stirred for 40 min at 25 °C. The resulting solution was filtered through Celite and concentrated under reduced pressure to ca. 3 mL. Heptane (8 mL) was added to precipitate the product as a very air sensitive solid in 69% yield (478 mg). Anal. Calcd for $C_{13}H_{23}P_2OIr$: C, 34.74; H, 5.16. Found: C, 34.55; H, 5.13. ^1H NMR (C_6D_6): δ 1.10, t ($^2J(P,H)$ = 3.4 Hz), PMe; 7.01, tt, 7.28, t, 7.46, dd, para, meta, and ortho H. ^{31}P NMR (C_6D_6): -24.4 ppm.

Dihydrogen Adducts of Vaska's Complex 1. Through a solution of **1** (0.05 mmol) in C_6D_6 (0.5 mL) at 25 °C in an NMR tube was bubbled H_2 (1 atm) for 5 min. The solution turned from yellow to colorless and the ^1H NMR spectrum was immediately recorded. The data reported in Table II show the spectral characteristics of the adducts which characterize the direction of addition in each case. The isomerization of **9** to **10** was most conveniently followed by ^{31}P NMR spectroscopy (see Table II). During the isomerization a peak was observed for $IrPh(CO)(PMe_3)_2$ at -24.4 ppm. Only one of these adducts, $[H_2ClIr(CO)(PMe_3)_2]$ was stable enough to analyze. Anal. Calcd for $C_7H_{20}P_2OClIr$: C, 20.50; H, 4.92. Found: C, 20.51; H, 4.84.

Other Adducts of 1b. Anhydrous HCl was bubbled into $[IrMe(CO)(PMe_3)_2]$ (**1b**, 13.9 mg, 0.036 mmol) in C_6D_6 (0.5 mL) in an NMR tube, and the ^1H NMR spectrum was recorded. Quantitative conversion to the known *cis,trans*-$[IrHCl_2(CO)(PMe_3)_2]$ was indicated by the spectral data: -17.08, t (J = 12.8 Hz), Ir-H; 1.28, t (J = 4.1 Hz), PMe.

To sample of **1b** (11 mg, 0.028 mmol) was added MeI (1.8 μL, 0.028 mmol). The ^1H NMR spectrum of the resulting colorless solution showed quantitative conversion to 1,2,6,4,3,5-$[IrMe_2I(CO)(PMe_3)_2]$: δ 0.49 and 0.51, t ($^3J(P,H)$ = 5.8 and 9 Hz), IrMe; 1.27, t (virtual coupling J_{app} = 3.8 Hz), PMe.

Acknowledgment. We wish to thank R. Hoffman (Cornell University) for discussions and the NSF for support.

Decamethylrhenocene, $(\eta^5\text{-}C_5Me_5)_2Re$

Judith A. Bandy,[1a] F. Geoffrey N. Cloke,*[,1b] Glyn Cooper,[1a] Jeremy P. Day,[1b] Reuben B. Girling,[1c] Robin G. Graham,[1d] Jennifer C. Green,[1a] Roger Grinter,[1d] and Robin N. Perutz[1c]

Contribution from the School of Chemistry and Molecular Sciences, University of Sussex, Brighton BN1 9QJ, U.K., the Department of Chemistry, University of York, York Y01 5DD, U.K., the School of Chemical Sciences, University of East Anglia, Norwich NR4 7TJ, U.K., the Inorganic Chemistry Laboratory, South Parks Road, Oxford OX1 3QR, U.K., and the Chemical Crystallography Laboratory, 9 Parks Road, Oxford OX1 3PD, U.K. *Received August 13, 1987*

Abstract: The synthesis of Cp^*_2ReH ($Cp^* = \eta^5\text{-}C_5Me_5$) from Re vapor and C_5Me_5H and its photochemical conversion into Cp^*_2Re are described. The X-ray crystal structure of the latter has been determined and shows the molecule to possess the parallel ring, eclipsed, sandwich structure (space group $P2_1/m$, a = 8.620 (3), b = 14.593 (5), c = 7.923 (3) Å, Z = 2, refinement on 1871 reflections, R_w = 0.037). The solid-state magnetic moment reveals Curie-Weiss behavior consistent with a $^2A_1$ (or $A_{1/2}$) ground state. Visible absorption and laser-induced fluorescence spectra in Ar and N_2 matrices showed a strong LMCT band with excellently resolved vibrational structure. The same transition is observed at room temperature in solution. Magnetic circular dichroism (MCD) spectra in Ar matrices show an intense signal with an inverse temperature dependence of intensity (C term). The value of $g_\parallel$ is determined from the magnetization curve of the MCD spectrum as 4.87 (19). Measurement of the ESR spectrum of Cp^*_2Re in frozen toluene at 4 K showed that the molecule also has an $E_{5/2}$ ground state under these conditions with $g_\parallel$ = 5.081 (3), A_{Re} = 1585 (3) MHz. The gas-phase photoelectron spectrum (He I and He II) proved inconsistent with an $E_{5/2}$ state for the neutral molecule and is best described by an equilibrium between $A_{1/2}$ and $E_{5/2}$ states. The value of the solution magnetic moment at room temperature (μ_{eff} = 1.95 (10) μ_B) also suggests an equilibrium between electronic states.

There is overwhelming evidence that the electronic structure of the metallocenes and other parallel sandwich complexes is well described by the ligand field model.[2-5] According to the LF model the d orbitals are split into three sets: in order of decreasing binding energy e_2 (xy, x^2-y^2), a_1 (z^2), and e_1 (xz,yz). (We use symbols indicating D_5 or D_6 symmetry, since various rotamers may be present.) When the complex has a d^5 configuration, the choice of electronic ground state is very sensitive to the particular combination of metal and ligand. Of the three possible configurations (Figure 1), the $^2A_1$ state is adopted by all the bis(arene) metal complexes,[6] while Cp_2Fe^+, $Cp^*_2Fe^+$, and Cp^*_2Mn adopt $^2E_2$ states ($Cp = \eta^5\text{-}C_5H_5$, $Cp^* = \eta^5\text{-}C_5Me_5$).[2-4,7,8] In contrast, Cp_2Mn and $(\eta^5\text{-}C_5H_4R)_2Mn$ either may be switched between $^2E_2$ and $^6A_1$ states by a change of host material or exhibit an equilibrium between them.[3,5,9] The $^2E_2$ state is subject to Jahn-Teller distortion which has been observed as both dynamic and static effects on the ESR spectra of manganocenes.[5,9] A significant distortion from D_{5d} symmetry has been established for Cp^*_2Mn in the crystal.[10]

In contrast to the first-row metallocenes, the d^5 configuration appeared until now to be highly unstable for third-row metallocenes. Thus the only metallocene characterized was rhenocene, Cp_2Re, formed by photolysis of Cp_2ReH in CO or N_2 matrices at ca. 20 K.[11] For a third-row metal, the $^2E_2$ state is subject to

(1) (a) University of Oxford. (b) University of Sussex. (c) University of York. (d) University of East Anglia.
(2) Warren, K. D. *Struct. Bonding (Berlin)* **1976**, *27*, 45.
(3) Green, J. C. *Struct. Bonding (Berlin)* **1981**, *43*, 37.
(4) Robbins, J. L.; Edelstein, N.; Spencer, B.; Smart, J. C. *J. Am. Chem. Soc.* **1982**, *104*, 1882.
(5) Ammeter, J. H. *J. Magn. Reson.* **1978**, *30*, 229.
(6) Cloke, F. G. N.; Dix, A. N.; Green, J. C.; Perutz, R. N.; Seddon, E. A. *Organometallics* **1983**, *2*, 1150. Bandy, J. A.; Berry, A.; Green, M. L. H.; Perutz, R. N.; Prout, K.; Verpeaux, J. N. *J. Chem. Soc., Chem. Commun.* **1984**, 729. Andrews, M. P.; Mattar, S. B.; Ozin, G. A. *J. Phys. Chem.* **1986**, *90*, 1037.
(7) Duggan, D. M.; Hendrickson, D. N. *Inorg. Chem.* **1975**, *14*, 955.
(8) Robbins, J. L.; Edelstein, N. M.; Cooper, S. R.; Smart, J. C. *J. Am. Chem. Soc.* **1979**, *101*, 3853.
(9) Ammeter, J. H.; Bucher, B.; Oswald, N. *J. Am. Chem. Soc.* **1974**, *96*, 7833. Ammeter, J. H.; Oswald, N.; Bucher, R. *Helv. Chim. Acta* **1975**, *58*, 671. Ammeter, J. H.; Zoller, L.; Bachmann, J.; Baltzer, P.; Gamp, E.; Bucher, R.; Deiss, E. *Ibid.* **1981**, *64*, 1063. Hebendanz, N.; Köhler, F. H.; Müller, G.; Riede, J. *J. Am. Chem. Soc.* **1986**, *108*, 3281.
(10) Freyberg, D. P.; Robbins, J. L.; Raymond, K. N.; Smart, J. C. *J. Am. Chem. Soc.* **1979**, *101*, 892.
(11) Chetwynd-Talbot, J.; Grebenik, P.; Perutz, R. N.; Powell, M. H. A. *Inorg. Chem.* **1983**, *22*, 1675. Cox, P. A.; Grebenik, P.; Perutz, R. N.; Graham, R. G.; Grinter, R. *Chem. Phys. Lett.* **1984**, *108*, 415.

0002-7863/88/1510-5039$01.50/0

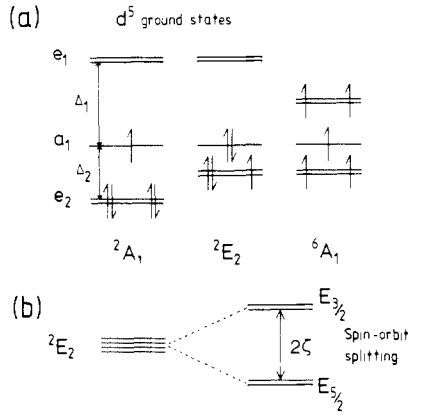

Figure 1. (a) The three possible electron configurations and terms available to d^5 parallel sandwich complexes in their ground states. (b) The effect of spin-orbit coupling on the $^2E_2$ term.

substantial spin-orbit coupling which splits it into $E_{5/2}$ and $E_{3/2}$ components (D_5* double group symmetry) separated by 2ζ (Figure 1b, ζ is the spin-orbit coupling constant). In the limit of no quenching of angular momentum by the ligands and perfect D_5* symmetry, we then expect g values of six (parallel) and zero (perpendicular).[2] In the double group formalism the $^2A_1$ state is symbolized by $A_{1/2}$ (this representation is sometimes given as $E_{1/2}$).

Rhenocene was shown to have the $E_{5/2}$ ground state by magnetic circular dichroism (MCD).[11] Photoelectron spectroscopy proved that the ground state of $[(\eta^5\text{-}C_5H_4Me)_2Os]^+$ was the same and provided a value of the $E_{5/2}$, $E_{3/2}$ energy separation of 0.62 eV (5000 cm^{-1}). The $A_{1/2}$ state lay 0.28 eV (2260 cm^{-1}) above the $E_{5/2}$ state.[12]

In this paper we demonstrate that Cp^*_2Re is a stable molecule prepared by UV photolysis of the hydride Cp^*_2ReH (cf. the transient Cp_2Re which has been obtained by photolysis of matrix isolated Cp_2ReH)[11]. Cp^*_2ReH itself is obtainable by cocondensation of rhenium vapor with C_5Me_5H; the synthetic aspects of this work have been briefly communicated.[13]

We report detailed studies of the electronic and molecular structure of Cp^*_2Re by X-ray diffraction, vibrational spectroscopy, UV-vis absorption and fluorescence, magnetic circular dichroism, electron spin resonance, photoelectron spectroscopy, and magnetic moments.

Experimental Section

All manipulations were carried out under an atmosphere of high purity nitrogen or in vacuo, with conventional Schlenck techniques, or in a Miller Howe drybox (<5 ppm H_2O, <1 ppm O_2). Solvents were dried and distilled before use by using standard procedures. Rhenium metal powder (99.9%) was vacuum melted prior to use in the cocondensation experiments. 1,2,3,4,5-Pentamethylcyclopentadiene was prepared by the method of Jutzi et al.[14] The metal vapor synthesis apparatus used in this work is of a type described elsewhere.[15] Mass spectra were recorded on a Kratos MS80 RF instrument. ^1H NMR spectra were recorded on a Bruker WM 360 at probe temperature; δ is relative to internal solvent. IR, UV-vis absorption, and laser-induced fluorescence spectra (LIF) were recorded in argon or nitrogen matrices at 12–20 K by using Perkin-Elmer 580 (±1 cm^{-1}), Perkin-Elmer Lambda 7G (±0.5 nm in visible spectrum), and Spex 1403 spectrometers (±2 cm^{-1}), respectively. The figures in parentheses give the absolute accuracy of the frequency or wavelength measurements. The fluorescence spectra were excited by a Spectra-Physics 170 Kr^+ laser. For these experiments, conducted at York, the matrix isolation apparatus, employing an Air-Products CS202 closed-cycle cooler is described in ref 16. The substrate for IR experiments was CsI, for UV-vis experiments LiF. Further UV-vis spectra and MCD spectra were recorded at the University of East Anglia with a new cryostat designed for MCD magnetization studies and capable of reaching 1.6 K and 10 T.[17] MCD spectra were recorded on a Cary 61 dichrograph and UV-vis spectra on a Cary 17D spectrometer, both interfaced to a microcomputer. The absorbance calibration of the Cary 17D was checked against standard samples. The ellipticity measurements on the Cary 61 were calibrated with a sample of optically pure D(+)-*n*-butylamine camphor sulfonate at 290 nm corrected for the relative sensitivity of the instrument at 590 and 290 nm. The latter was established by using Stephens' method with a quarter-wave plate and linear polarizer.[18] Samples for matrix isolation were deposited from a side-arm heated to ca. 333–343 K. It proved most effective to use a side-arm without stopcock since Cp^*_2Re is very soluble in vacuum grease. Research grade gases were obtained from B.O.C. or Messer-Griesheim.

Raman spectra of solid Cp^*_2Re were recorded on a thin sublimate in glass capillaries by using the microscope attachment (40 × objective on Nikon microscope with BGSC collection optics) of the Spex 1403 spectrometer and Kr^+ or Ar^+ laser excitation. Typically the laser power was 10 mW at the sample; resolution was 5 cm^{-1}. Spectra were recorded digitally at 1-cm^{-1} steps, 1-s integration with the Spex Scamp computer. Up to eight scans were added together; following subtraction of the background, the data were smoothed digitally (7 point).

He I and He II photoelectron spectra (PES) of Cp^*_2Re were recorded on a P.E.S. Laboratories 0078 spectrometer interfaced with a Research Machines 380Z microcomputer at a resolution of approximately 80 meV. Better resolution than this could not be obtained as the compound had a deleterious effect on instrumental performance. The temperature range used for data collection was 88–100 °C.

The CI calculations were performed by diagonalization of the matrices with a computer program run on a Research Machines Nimbus microcomputer.

Magnetic susceptibility measurements on crystalline Cp^*_2Re were made in Berkeley on a SHE905 SQUID magnetometer. The susceptibility was determined at fields of 0.1, 0.5, 1.0, 2.0, and 4.0 T between 5 and 300 K. The solution magnetic moment was determined by Evans method,[19] employing a 5-mm coaxial cell and by using TMS in C_6D_6 as the reference signal.

Synthesis of Cp^*_2ReH. In a typical experiment, rhenium vapor (7.61 g, 41 mmol) from a premelted ingot (ca. 24 g), heated to ca. 3200 °C with an electron beam power input of 3.3 kW, was cocondensed with an excess of 1,2,3,4,5-pentamethylcyclopentadiene (85 g, 540 mmol) in a liquid nitrogen cooled 50 L reactor over a period of 3 h. After warming up to room temperature, the product was extracted from the apparatus with THF (1 L). The mixture was then filtered through a bed of Celite, and THF and excess pentamethylcyclopentadiene were removed in vacuo. The resultant brown oil was redissolved in THF (200 cm^3) and treated with 1 M aqueous HCl (200 cm^3). The THF was then removed in vacuo, and the resultant orange aqueous solution of $[Cp^*_2ReH_2^+][Cl^-]$ was filtered through a Celite bed. Addition of 1 M aqueous NaOH (210 cm^3) precipitated crude Cp^*_2ReH which was collected, washed with water, and dried in vacuo. Finally, chromatography on deactivated alumina (4% H_2O w/w, 2:1 hexane–ether eluant) afforded Cp^*_2ReH as yellow crystals (2.05 g, 4.5 mmol; yield 11% based on rhenium). The compound may be recrystallized from pentane at −78 °C but is sufficiently pure for direct conversion into Cp^*_2Re.

Synthesis of Cp^*_2Re. Cp^*_2ReH (2.05 g, 4.5 mmol) was dissolved in pentane (50 cm^3) in a glass ampoule equipped with a greaseless stopcock and photolyzed (500 W medium pressure Hg arc) for 100 h. The resultant deep purple solution was filtered, concentrated, and cooled to −78 °C, affording deep purple crystals of Cp^*_2Re (1.19 g, 2.3 mmol, 60%): MS, m/e 456 (M^+) mol wt (vapor pressure equilibration), 450. ^1H NMR (C_6D_6) 30.8 δ ($\nu_{1/2}$ = 560 Hz). Anal. Calcd for $C_{20}H_{30}Re$: C, 52.75; H, 6.59. Found: C, 53.02; H, 6.34.

X-ray Data Collection. Crystals of Cp^*_2Re were sealed under N_2 in Lindemann glass capillaries. One crystal (0.4 × 0.25 × 0.475 mm) was mounted on an Enraf-Nonius CAD-4 diffractometer at room temperature for data collection by using graphite-monochromated Mo Kα radiation. Cell dimensions were obtained by least-squares methods from the positions of 25 carefully centered reflections. Crystal data and scan conditions are listed in Table I. Data were collected in the zone $+h,+k,\pm l$, and systematic absences were found to be $0k0$ with k odd. During data reduction correction was made for Lorentz, polarization, and absorption effects.[20]

(12) Evans, S.; Green, M. L. H.; Jewitt, B.; Orchard, A. F.; Pygall, C. F. *J. Chem. Soc., Faraday Trans. 2* **1978**, *68*, 1847.
(13) Cloke, F. G. N.; Day, J. P. *J. Chem. Soc., Chem. Commun.* **1985**, 967.
(14) Kohl, F. X.; Jutzi, P. *J. Organomet. Chem.* **1983**, *243*, 119.
(15) Cloke, F. G. N.; Green, M. L. H. *J. Chem. Soc., Dalton Trans.* **1981**, 1938.
(16) Chetwynd-Talbot, J.; Grebenik, P.; Perutz, R. N. *Inorg. Chem.* **1982**, *21*, 3647. Haddleton, D. M.; McCamley, A.; Perutz, R. N. *J. Am. Chem. Soc.* **1988**, *110*, 1810.
(17) Graham, R. G.; Grinter, R.; Stern, D. R.; Timms, K. *J. Phys. E.* **1986**, *19*, 776.
(18) Osborne, G. A.; Cheng, J. C.; Stephens, P. J. *Rev. Sci. Inst.* **1973**, *44*, 10.
(19) Evans, D. F. *J. Chem. Soc.* **1959**, 2005.

Table I. Crystal Data and Scan Conditions

formula	$C_{20}H_{30}Re$
mol wt	456.66
space group	$P2_1/m$
a, Å	8.620 (3)
b, Å	14.593 (5)
c, Å	7.923 (3)
β, deg	106.07 (3)
Z	2
cell vol, Å^3	957.7
d_{calcd}, g cm^{-3}	1584
$F(000)$	450
μ (Mo Kα), cm^{-1}	64.2
λ (Mo Kα_1), Å	0.70930
transmission factors	1, 2.185
scan speed, deg min^{-1}	1.8–5.5
scan mode	$\omega - 2\theta$
scan width, deg	1.2 + 0.35 tanθ
$2\theta_{max}$, deg	55
measd reflctns	3169
obsd reflctns [$I > 3\sigma(I)$]	1871
R_{merge}	0.039
R	0.034
R_w	0.037

X-ray Structure Solution and Refinement. The structure was solved by the heavy atom method and refined by full-matrix least squares. Hydrogen atoms were located from difference Fourier syntheses and refined with geometrical restraints[21] and with U[iso] fixed at 0.1 Å. All non-hydrogen atoms were refined with anisotropic vibration coefficients. C(4) was found to have physically unreasonable temperature factors when constrained to lie in the mirror plane and was allowed to refine off. All methyl carbon atoms exhibited high thermal motion suggesting some degree of positional disorder (as found for decamethylruthenocene and decamethylosmocene[22]). The C–Me bond lengths were restrained to 1.505 (5) Å, appropriate for a Csp^2–Csp^3 bond.[23] Correction was made for anomalous dispersion[24] and a modified Chebyshev weighting scheme was applied[25] where

$$w = 1/\sum_{r=1}^{n} A_r T_r(X) \quad \text{and} \quad X = F_o/|F_o|_{max}$$

T_r is the polynomial function with coefficients 60.41, −61.46, and 42.59 to give satisfactory agreement analyses. At convergence

$$R = \sum||F_o| - |F_c||/\sum|F_o| = 0.034 \quad \text{and}$$

$$R' = [w(|F_o| - |F_c|)^2/\sum w|F_o|^2]^{1/2} = 0.037$$

Solution and refinement used the Oxford CRYSTALS package[26] on the VAX 11/750 computer of the Chemical Crystallography Laboratory Oxford University. Scattering factors were taken from *International Tables for X-ray Crystallography*.[27]

Results

Synthesis. By using an apparatus described elsewhere, rhenium atoms were cocondensed with 1,2,3,4,5-pentamethylcyclopentadiene (Cp*H) and the compound Cp^*_2ReH could be isolated from the reaction mixture in 10–15% yield. The most convenient isolation procedure involved treatment of the reaction mixture with dilute acid to afford an aqueous solution of the cation $Cp^*_2ReH_2^+$ (thus separating the organometallic product from organic impurities) which could readily be deprotonated to give the neutral monohydride. Cp^*_2ReH is a yellow, volatile, air-sensitive crystalline solid, extremely soluble in hydrocarbon solvents, whose spectroscopic properties have been reported in an earlier communication.[13]

UV irradiation of a pentane solution of Cp^*_2ReH produced a rapid color change from yellow to purple. From the solution could be obtained deep purple crystals of Cp^*_2Re in ca. 60% isolated yield, although the extreme solubility of the compound rendered mechanical losses unavoidable. Cp^*_2Re is a thermally stable, air-sensitive, purple crystalline solid which is monomeric in solution and in the gas phase.

X-ray Crystal Structure of Cp^*_2Re. The molecular structure is shown in Figure 2 with atomic labels, atomic coordinates are listed in Table II, and bond distances and angles are found in Table III.

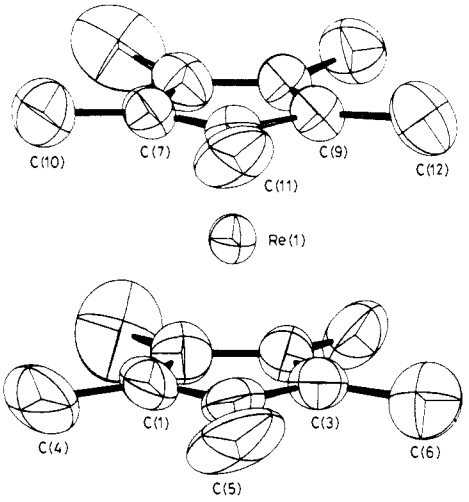

Figure 2. The structure of Cp^*_2Re showing thermal ellipsoids drawn at the 50% probability level. Hydrogen atoms have been omitted for clarity, and only one position is shown for C(4).

Table II. Atomic Coordinates and Equivalent Isotropic Temperature Factors for Cp^*_2Re

atom	x/a	y/b	z/c	U (equiv)
Re(1)	0.20895 (3)	0.2500	0.41751 (4)	0.0468
C(1)	0.406 (1)	0.2500	0.667 (1)	0.0749
C(2)	0.3096 (9)	0.1713 (5)	0.6654 (8)	0.0692
C(3)	0.1531 (7)	0.2022 (4)	0.6625 (7)	0.0620
C(4)	0.584 (1)	0.252 (7)	0.683 (2)	0.1197
C(5)	0.362 (2)	0.0724 (7)	0.676 (2)	0.1183
C(6)	0.011 (1)	0.1444 (7)	0.673 (1)	0.0885
C(7)	0.2876 (9)	0.2500	0.173 (1)	0.0647
C(8)	0.1901 (8)	0.1717 (4)	0.1712 (8)	0.0635
C(9)	0.0351 (6)	0.2008 (3)	0.1688 (7)	0.0509
C(10)	0.459 (1)	0.2500	0.159 (2)	0.1009
C(11)	0.240 (2)	0.0736 (6)	0.160 (1)	0.1004
C(12)	−0.1114 (9)	0.1424 (6)	0.157 (1)	0.0811
H(1)	0.60 (3)	0.30 (1)	0.59 (2)	0.1000
H(2)	0.61 (3)	0.186 (9)	0.64 (2)	0.1000
H(3)	0.66 (1)	0.26 (1)	0.80 (1)	0.1000
H(4)	0.297 (8)	0.031 (5)	0.606 (8)	0.1000
H(5)	0.401 (8)	0.047 (5)	0.801 (9)	0.1000
H(6)	0.456 (8)	0.085 (5)	0.631 (8)	0.1000
H(7)	−0.090 (8)	0.164 (5)	0.597 (8)	0.1000
H(8)	0.044 (9)	0.084 (5)	0.630 (8)	0.1000
H(9)	0.002 (8)	0.136 (5)	0.796 (9)	0.1000
H(10)	0.45 (1)	0.2500	0.04 (1)	0.1000
H(11)	0.514 (6)	0.197 (4)	0.214 (6)	0.1000
H(12)	0.205 (8)	0.050 (5)	0.039 (9)	0.1000
H(13)	0.197 (8)	0.034 (5)	0.238 (8)	0.1000
H(14)	0.354 (9)	0.074 (5)	0.200 (7)	0.1000
H(15)	−0.173 (8)	0.132 (4)	0.036 (9)	0.1000
H(16)	−0.180 (8)	0.174 (5)	0.221 (8)	0.1000
H(17)	−0.077 (8)	0.085 (5)	0.212 (8)	0.1000

(20) North, A. C. T.; Phillips, D. C.; Mathews, F. S. *Acta Crystallogr., Sect. A: Cryst. Phys., Diffr., Theor. Gen. Crystallogr.* **1968**, *24*, 351. *International Tables for X-ray Crystallography*; Kynoch Press: Birmingham, England, 1959; Vol. II, p 302.
(21) Waser, J. T. *Acta Crystallogr.* **1963**, *16*, 1091. Rollet, J. S. *Crystallographic Computing*; Ahmed, F. R., Ed.; Munksgaard, Copenhagen, 1969; p 169.
(22) Albers, M. O.; Liles, D. C.; Robinson, D. J.; Shaver, A.; Singleton, E.; Wiege, M. B.; Boeyens, J. C. A.; Levendis, D. C. *Organometallics* **1986**, *5*, 2321.
(23) *Tables of Interatomic Distances and Configuration in Molecules and Ions*; Sutton, L. E., Ed.; Chemical Society: London, 1965; p S 15s.
(24) *International Tables for X-ray Crystallography*; Kynoch Press: Birmingham, England, 1974; Vol. IV, p 149.
(25) Carruthers, J. R.; Watkin, D. J. *Acta Crystallogr., Sect. A: Cryst. Phys., Diffr., Theor. Gen. Crystallogr.* **1979**, *35*, 698. Prince, E. *Mathematical Techniques in Crystallography*; Springer-Verlag: New York, 1982.
(26) Watkin, D. J.; Betteridge, P. W.; Carruthers, J. R. CRYSTALS *User Manual*; Oxford University Computing Laboratory: Oxford, U.K., 1986.
(27) Reference 24, p 99.

Table III. Bond Lengths (Å) and Angles (deg) for Cp^*_2Re

	Re(1)-C(1)	2.223 (8)	
	Re(1)-C(2)	2.233 (6)	
	Re(1)-C(3)	2.237 (5)	
	Re(1)-C(7)	2.222 (8)	
	Re(1)-C(8)	2.228 (6)	
	Re(1)-C(9)	2.238 (5)	
C(1)-C(2)	1.418 (9)	C(2')-C(1)-C(2)	108.2 (7)
C(1)-C(4)	1.505 (5)	C(2)-C(1)-C(4)	127 (4)
C(2)-C(3)	1.417 (9)	C(2')-C(1)-C(4)	125 (4)
C(2)-C(5)	1.506 (5)	C(1)-C(2)-C(3)	107.3 (6)
C(3)-C(3')	1.395 (13)	C(1)-C(2)-C(5)	127.6 (8)
C(3)-C(6)	1.506 (4)	C(5)-C(2)-C(3)	125.0 (8)
		C(2)-C(3)-C(3')	108.6 (4)
		C(2)-C(3)-C(6)	127.1 (7)
		C(6)-C(3)-C(3')	124.1 (5)
C(7)-C(8)	1.416 (8)	C(8')-C(7)-C(8)	107.6 (6)
C(7)-C(10)	1.507 (5)	C(8)-C(7)-C(10)	126.1 (3)
C(8)-C(9)	1.397 (8)	C(7)-C(8)-C(9)	108.5 (5)
C(8)-C(11)	1.504 (4)	C(7)-C(8)-C(11)	126.2 (7)
C(9)-C(9')	1.437 (10)	C(9)-C(8)-C(11)	125.1 (7)
C(9)-C(12)	1.505 (4)	C(8)-C(9)-C(9')	107.7 (3)
		C(8)-C(9)-C(12)	127.7 (6)
		C(12)-C(9)-C(9')	124.5 (4)

Each molecule of Cp^*_2Re exhibits a crystallographic mirror plane passing through Re(1), C(1), C(7), C(10) and bisecting the C(3)-C(3') and C(9)-C(9') bonds (primes denote atoms related by the mirror, x, $^1/_2 - y$, z). The two cyclopentadienyl rings are planar and parallel with the methyl groups deviating from the ring mean planes by 0.069-0.124 Å away from rhenium. The conformation is eclipsed as found for decamethylruthenocene and decamethylosmocene but in contrast to the staggered arrangement of the rings observed in decamethylmanganocene and decamethylferrocene.[28] Rhenium is found to be 1.882 and 1.880 Å from the mean planes of the two rings and this large separation of the two rings prevents unfavorable methyl-methyl contacts in the eclipsed conformation. The closest $C(H_3)\cdots C(H_3)$ approach between the rings is for C(6)···C(12) of 3.927 Å.

Although the reflection data appear to be of good quality, the possible rotational disorder of the pentamethylcyclopentadienyl rings and the presence of rhenium as the dominant X-ray scatterer prevents detailed analysis and comparison of the ring geometries with similar compounds. However, the Csp^2-Csp^2 bond distances show some deviation from perfect D_{5h} symmetry, as seen in $CpRe(CO)_3$[29] which would have been expected to have cylindrical symmetry. The Re-Csp^2 distances are longer in this latter compound than observed in Cp^*_2Re due to the electron-withdrawing nature of the carbonyl ligands but for Cp^*_2Re appear within the range found for other rhenium-cyclopentadienyl derivatives.[30] The structure of rhenocene itself is, as yet, unknown.

The methyl groups are arranged with two hydrogens toward the metal and one away. This arrangement seems to maximize all H···H contacts, both within the ring and between rings. Molecular packing appears to be similar to that observed for the ruthenium and osmium analogues. The cyclopentadienyl rings are approximately parallel to the ab plane forming interlocking layers along the [100] axis.

Infrared and Raman Spectra. The IR spectrum of Cp^*_2Re matrix-isolated in argon at 20 K is dominated by clusters of ligand modes (Figure 3, Table IV) at ca. 2900, 1450, and 1030 cm^{-1}. Three low-frequency bands give information about the skeletal modes. Additional data on the ground-state vibrations of matrix-isolated Cp^*_2Re is forthcoming from the laser-induced fluorescence spectrum (see below).

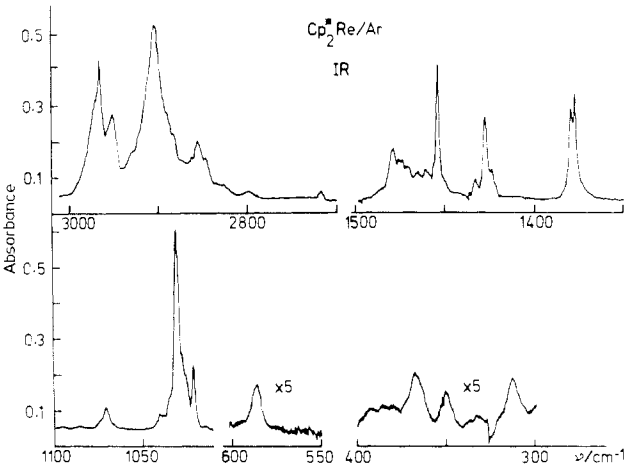

Figure 3. The IR spectrum of Cp^*_2Re in an argon matrix at 20 K. Any bands in the regions not illustrated are considerably weaker than those shown (deposition time 390 min, sample temperature 334-343 K, 13.6 mmol Ar deposited).

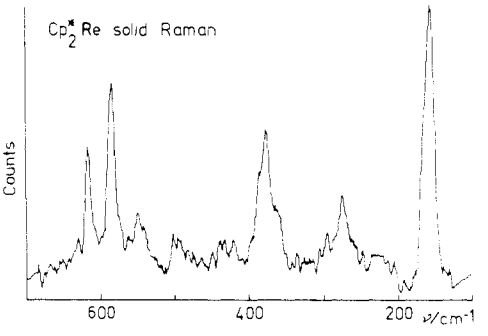

Figure 4. Raman spectrum of solid Cp^*_2Re at 300 K measured on thin film of sublimate with microscope attachment (excitation wavelength 647.1 nm, slit 6 cm^{-1}, power at sample 10 mW, averaged from eight 8 scans; the rising background has been subtracted, and the spectrum has been smoothed digitally (7 point)).

Table IV. Vibrational Spectra of Cp^*_2Re ($\bar{\nu}/cm^{-1}$)

IR Ar matrix	IR solid film at 12 K	Raman solid at 300 K
2965 s	2960 s	
2950 s	2945 s	
2902 s	2900 s	
2856 m	2848 sh	
2796 w		
2717 w		
1479 m	1474 m	
1475 m, b		
1470 m, b		
1465 m, b		
1460 m, b		
1454 s	1452 m	
1433 w		
1427 s	1422 m	1417 m
1379 s	1376 s	
1377 s		
1071 w	1070 w	
1040 sh		
1031 s	1030 s	
1022 m		616 m
586 w	587 w	583 m
367 w	367 w	378 m
350 w		360 sh
313 w		
		273 m
		160 s

The IR spectrum of *solid* Cp^*_2Re at 12 K obtained by evaporating argon from the matrix appears to be a very broad version of the matrix spectrum (Table IV). The Raman spectrum of *solid* Cp^*_2Re was obtained by 647.1-nm excitation with a microscope.

(28) Freyberg, D. P.; Robbins, J. L.; Raymond, K. N.; Smart, J. C. *J. Am. Chem. Soc.* **1979**, *101*, 892.
(29) Fitzpatrick, P. J.; Le Page, Y.; Butler, I. S. *Acta Crystallogr., Sect. B: Struct. Crystallogr. Cryst. Chem.* **1981**, *37*, 1052.
(30) Prout, K.; Cameron, T. S.; Forder, R. A.; Critchley, S. R.; Denton, B.; Rees, G. V. *Acta Crystallogr., Sect. B: Struct. Crystallogr. Cryst. Chem.* **1974**, *30*, 2290. Alcock, N. W. *J. Chem. Soc. A* **1967**, 2001.

Table V. Visible Absorption Band Maxima of Cp^*_2Re in Argon Matrix Before Annealing[b]

progression A[a] $T_0 + n(390.6 \pm 2.6)$ cm^{-1}			progression A[a] after annealing $T_0 + n(387.5 \pm 3.0)$ cm^{-1}			progression B[a] $T_0 + 124 + n(391.3 \pm 2.2)$ cm^{-1}			progression B[a] after annealing $T_0 + 141 + n(391.8 \pm 0.4)$ cm^{-1}			progression C $T_0 + 968 + n(394 \pm 2.7)$ cm^{-1}			progression D $T_0 + 1023 + n(390.5 \pm 4)$ cm^{-1}		
nm	cm^{-1}	interval cm^{-1}	nm	cm^{-1}	interval cm^{-1}	nm	cm^{-1}	interval cm^{-1}	nm	cm^{-1}	interval cm^{-1}	nm	cm^{-1}	interval cm^{-1}	nm	cm^{-1}	interval cm^{-1}
603.3	16576	393	603.6	16567	391	598.8	16700	394	598.5	16708	392	570.0	17544	396	568.2	17599	393
589.3	16969	389	589.7	16958	385	585.0	17094	392	584.8	17100	392	557.4	17940	395	555.8	17992	390
576.1	17358	391	576.6	17343	385	571.9	17486	390	571.7	17492	391	545.4	18335	395	544.0	18382	394
563.4	17749	393	564.1	17727	389	559.4	17876	389	559.2	17883	392	533.9	18730	390	532.6	18776	385
551.2	18142	387	552.0	18116		547.5	18265		547.2	18275	392	523.0	19120		521.9	19161	
539.7	18529	(375)							535.7	18667							
(529.0)	(18904)																

[a] Only the most intense components of progressions A and B are quoted (see Table VI). [b] For each progression a summarizing expression is given in addition to observed frequencies.

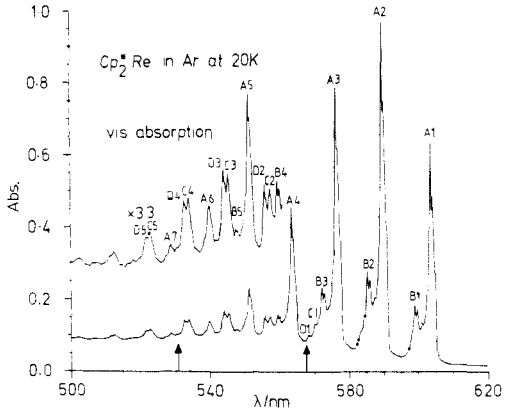

Figure 5. Visible absorption spectrum of Cp^*_2Re in an argon matrix at 20 K. The inset shows the spectrum under a 3.3 times ordinate expansion. The heavy arrows mark the laser wavelengths used for fluorescence excitation. The features are coded A1, A2, etc. as in Tables II and III (deposition time 100 min, sample temperature 333 K, 3.1 mmol Ar deposited, slits 0.25 nm, scan speed 0.125 nm s^{-1}).

Unlike $Cp^*_2Fe^+$ salts,[7] there was no evidence for resonance enhancement on changing the excitation wavelength. However, the skeletal modes are now the most intense in the spectrum with a striking band at 160 cm^{-1} (Figure 4, Table IV).

Ultraviolet–Visible Absorption Spectra. The UV–vis absorption spectrum of Cp^*_2Re *matrix-isolated* in argon showed broad maxima at 276 (sh) and 265 nm and an exceptionally sharp band with excellently resolved fine structure in the visible (Figure 5, Table V). The most conspicuous features arise from a progression with its first component at 603.3 nm (16 576 cm^{-1}, taken as T_0) and a vibrational interval of 391 ± 3 cm^{-1} (taken from the first six components). A second progression (progression B $\bar{\nu} = T_0 + 140 + n\nu'$ cm^{-1}, $\nu' = 391 \pm 2$ cm^{-1}) grew at the expense of the first progression after annealing to 35 K and recooling to 12 K (Table VI). The two progressions are presumed to arise from different matrix sites. After annealing the revised values for progression A were $T_0 = 16\,567$ cm^{-1} $\nu' = 388 \pm 3$ cm^{-1} and for progression B, T_0 16 708 cm^{-1}, $\nu' = 391.8 \pm 0.4$ cm^{-1}. Two further much weaker progressions in the same vibration were detected most conspicuously before annealing. The most likely origins for them are 17940 cm^{-1} ($T_0 + 968$ cm^{-1}) and 17992 cm^{-1} ($T_0 + 1023$ cm^{-1}). Thus we are able to identify three excited state vibrations 392, 968, and 1023 cm^{-1}.

Each of the major components of the spectrum also exhibited fine structure which changed significantly on annealing (Figure 6). The component intervals average at 19.2 ± 2.4 cm^{-1} on progression A and 23.5 ± 1.0 cm^{-1} on progression B. Such structure has been observed previously in the spectra of matrix-isolated metallocenes but has never been so clearly resolved.[11,16] It is almost certainly associated with coupling to matrix phonon modes in the electronically excited state. The most intense phonon mode of solid argon is observed at 32.4 cm^{-1} with weaker bands at ca. 15, 50, and 72 cm^{-1}.[31]

(31) Knözinger, E.; Wittenbeck, R. *J. Am. Chem. Soc.* **1983**, *105*, 2154.

Table VI. Visible Absorption Band Maxima of Cp^*_2Re in Argon Matrix[a]

	nm	cm^{-1}	interval		nm	cm^{-1}	interval
	604.4	16545	22		599.4	16683	25
A1	603.6	16567	17	B1	598.5	16708	23
	603.0	16584			597.7	16731	
	590.4	16938	20		585.6	17077	23
A2	589.7	16958	20	B2	584.8	17100	23
	589.0	16978			584.0	17123	
	577.2	17325	18		572.4	17470	22
A3	576.6	17343	22	B3	571.7	17492	24
	576.2	17355	22		570.9	17516	
	575.8	17367					
	564.1	17727	16		559.9	17860	23
A4	563.6	17743	16	B4	559.2	17883	25
	563.1	17759			558.4	17908	

[a] Fine structure on progressions A and B after annealing to 35 K and recooling to 12 K. Mean intervals: $\bar{\nu}_A = 19.2 \pm 2.4$ cm^{-1}; $\bar{\nu}_B = 23.5 \pm 1.0$ cm^{-1}.

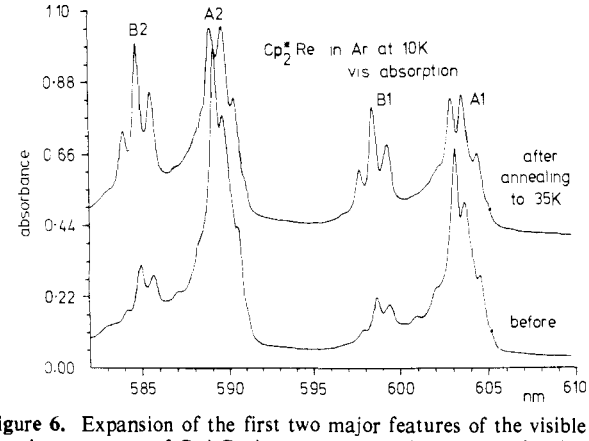

Figure 6. Expansion of the first two major features of the visible absorption spectrum of Cp^*_2Re in an argon matrix at 12 K, showing the two sites A and B. Lower spectrum: before annealing. Upper spectrum; after annealing to 35 K and recooling to 12 K (deposition and spectral conditions, as in Figure 4).

Arguing that there should be a substantial change in the phonon structure,[31] we isolated Cp^*_2Re in an N_2 matrix. The major progression frequency remained at 388.8 ± 3.1 cm^{-1}. To our surprise, very little phonon structure was apparent on deposition. However, its absence facilitated the identification of minor progressions with origins at ($T_0 + 707$), ($T_0 + 966$), and ($T_0 + 1024$) cm^{-1} (Table VII). The effect of annealing was far less striking than in argon, but it did bring out structure on the first progression with components separated by an average of 16 ± 2 cm^{-1} (average interval on A1, A2), an interval barely less than for the corresponding progression in argon.

The optical spectrum of Cp^*_2Re in toluene solution is close to the matrix spectrum. Although each band is much broader, vibrational structure is still detected and can be brought out by cooling and by recording as a second derivative (Figure 7, Table

Table VII. Visible Absorption Band Maxima of Cp^*_2Re in Nitrogen Matrix Before Annealing[a]

progression A $T_0 + n(388.8 \pm 3.1)$ cm^{-1}			fine structure on first two components of progression A			progression B $T_0 + 128 + n(390.2 \pm 2.9)$ cm^{-1}			progression E $T_0 + 707 + n(392 \pm 2)$ cm^{-1}			progression C $T_0 + 966 + n(393 \pm 4)$ cm^{-1}			progression D $T_0 + 1024 + n(389 \pm 5)$ cm^{-1}		
nm	cm^{-1}	interval cm^{-1}	nm	cm^{-1}	interval cm^{-1}	nm	cm^{-1}	interval cm^{-1}	nm	cm^{-1}	interval cm^{-1}	nm	cm^{-1}	interval cm^{-1}	nm	cm^{-1}	interval cm^{-1}
602.2	16 606		602.8	16 589		597.6	16 734		577.6	17 313		569.1	17 572		567.2	17 630	
		389			17			389			392			397			388
588.4	16 995		602.2	16 606		584.0	17 123		564.8	17 705		556.5	17 969		555.0	18 018	
		390			16			390			391			393			391
575.2	17 385		601.6	16 622		571.0	17 513		552.6	18 096		544.6	18 362		543.2	18 409	
		390						395			395			393			395
562.6	17 775		589.0	16 978		558.4	17 908		540.8	18 491		533.2	18 755		531.8	18 804	
		387			17			387			391			387			382
550.6	18 162		588.4	16 995		546.6	18 295		529.6	18 882		522.4	19 142		521.2	19 186	
		384			12			390									
539.2	18 546		588.0	17 007		535.2	18 685										
		393															
528.0	18 939																

[a] For each progression a summarizing expression is given in addition to the observed frequencies.

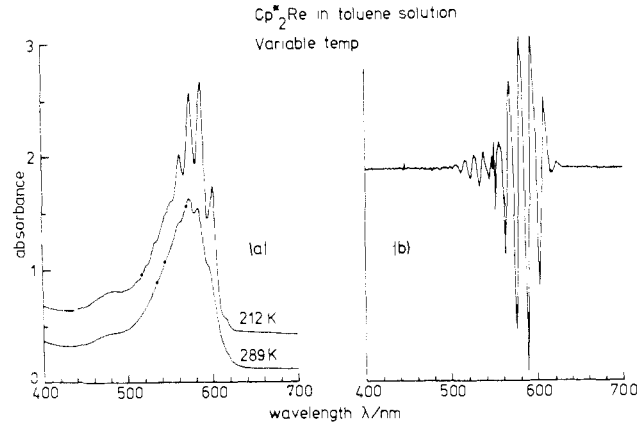

Figure 7. (a) Visible, absorption spectrum of Cp^*_2Re in toluene solution at 212 and 289 K. (b) Second derivative of the spectrum at 212 K. The maxima in absorption corresponds to the minima below the axis.

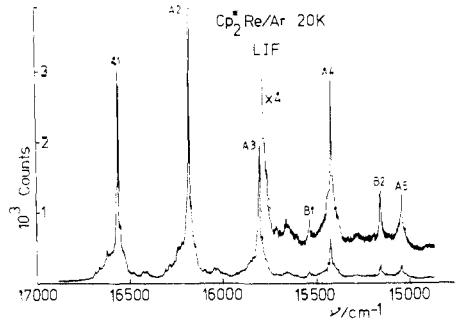

Figure 8. Laser-induced fluorescence spectrum of Cp^*_2Re in argon matrix at 20 K. The inset shows a four times ordinate expansion (excitation wavelength 568.2 nm, power 50 mW, slits 5 cm^{-1}, deposition time 74 min, sample temperature 333 K, 2.0 mmol Ar deposited).

Table VIII. Visible Absorption Spectrum of Cp^*_2Re in Toluene Solution at 212 K

nm	cm^{-1}	interval/cm^{-1}
616.0	16234	
		399
601.2	16633	
		380
587.8	17013	
		367
574.8	17380	
		388
562.8	17768	
		374
551.2	18142	
		244
544.8	18382	
		415
534.0	18727	
		360
524.0	19084	
480	20833	

VIII). The origin is red-shifted 460 cm^{-1} with respect to an argon matrix, and the progression frequency averages 382 cm^{-1} (first five components). Interestingly, we found a shoulder at 480 nm, which is not associated with oxidation. If this feature is present at all in the matrix spectrum, it must remain very broad. We recorded the solution spectrum between 212 and 343 K and found that the width of the vibrational components increased reversibly with temperature, but there were no signs of any equilibria between excited states. We checked that Cp^*_2Re has no near IR absorption band in solution between 2100 and 1800 and between 1650 and 700 nm with extinction coefficient greater than 0.3% of the visible band.

Laser-Induced Fluorescence Spectra. When a sample of Cp^*_2Re matrix-isolated in argon was irradiated into the tail of the (3-0) component of progression B without annealing (568.2 nm, 50 mW, see Figure 5), a sharp, intense emission progression was observed. The origin was at 16 574 cm^{-1} only 2 cm^{-1} from the measured position of T_0 in the absorption spectrum (Figure 8). There can be no doubt that this is the 0–0 band. Thus irradiation into the *second* site results in emission from the *first* site. The main emission progression has frequency 383.3 ± 1.0 cm^{-1} (Table IX), 7.3 cm^{-1} lower than the corresponding excited state progression. The values for the first members of the progression are somewhat

Table IX. Laser-Induced Fluorescence Spectra of Cp^*_2Re in Argon Matrix (cm^{-1})[a] Excited at Laser Wavelengths (Frequencies) Specified[b,c]

progression A[b] $T_0 - n(383.3 \pm 1.0)$ cm^{-1}		progression B[b] $T_0 - 1033 - n(383.7)$ cm^{-1}		progression A[c] $T_0 - n(383.0 \pm 0.7)$ cm^{-1}		progression B[c] $T_0 - 1034 - n(383.5 \pm 0.6)$ cm^{-1}	
$\bar{\nu}$	interval	$\bar{\nu}$	interval	$\bar{\nu}$	interval	$\bar{\nu}$	interval
16574	384	15539	384	16573	384	15539	383
16190	384	15155	383	16189	383	15156	384
15806	383	14772	384	15806	383	14772	384
15423	382	14388		15423	382	14388	383
15041	(381)			15041	383	14005	
(14660)				14658			

[a] For each progression a summarizing expression is given in addition to the observed frequencies. [b] λ_{ex} = 568.2 nm. $\bar{\nu}_{ex}$ = 17599 cm^{-1}. [d] λ_{ex} = 530.9 nm. $\bar{\nu}_{ex}$ = 18836 cm^{-1}.

Table X. Magnetic Circular Dichroism of $Cp_2{}^*Re$ in Argon Matrices[a]

nm	ΔA	nm	ΔA
296	-	246	+
279	+	232	-
257	+		

[a] UV bands.

higher and differ by 9 cm^{-1} (ν' = 393, ν'' = 384 cm^{-1}). A second much weaker progression in the same frequency was observed to start at T_0 = 1033 cm^{-1} (cf. progression D in absorption, ν' = 1023 cm^{-1}). Very weak features were also observed on either side of the main bands.

Proof that the emission originates in fluorescence rather than the resonance Raman effect is achieved by changing the excitation wavelength to 530.9 nm, which caused a shift in the absolute frequency of the major peaks of $\leq$1 cm^{-1} (Table IX). However, there was an increase in intensity of the weak components on the side of each band suggesting that these bands arise from minor sites.

Surprisingly, Cp^*_2Re (in toluene solution) even fluoresces weakly at room temperature, with an emission maximum at 605 nm and an excitation maximum at 550 nm.

Magnetic Circular Dichroism (MCD). The MCD spectrum of Cp^*_2Re in an argon matrix, measured at ±5 T and 1.8 K (Figure 9), showed the structured peak near 600 nm as a very intense feature with positive ΔA. The positions of the maxima were in excellent agreement with the absorption spectrum and are not tabulated. The UV region provided considerable extra information principally because of the changing sign of the dichroism (Table X).

The inverse temperature variation of the MCD signal demonstrates that the spectrum arises from the C term of a paramagnetic molecule. Furthermore, the MCD provides the opportunity of estimating $g_\parallel$ for Cp^*_2Re either from the ratio of integrated differential absorbance to integrated absorbance ($\Delta A/A$) or from the shape of the magnetization curve, i.e., from the variation of differential absorbance with B/T. We have used both methods, although we consider the latter to be far more satisfactory. The magnetization method will be discussed in more detail elsewhere.[32]

Using the analysis developed previously for Cp_2Re with an $E_{5/2}$ ground state, the parallel component of the g value is given by[11]

$$g_\parallel = 11.92 \frac{T}{B} \frac{\Delta A}{A}$$

where B, the magnetic flux density, is measured in Tesla. The experimental value of $\Delta A/A$ of 0.49 ± 0.13 at 10.9 K and 3.0 T gives a value of $g_\parallel$ = 5.3 ± 1.4. At this value of B/T no correction for saturation is required (see below). The main source of error lies in the estimate of integrated absorbance since the maximum value was only 0.09 and is observed against an undulating background resulting from interference fringes. Our calibration procedure has been described in the Experimental Section.

The magnetization curve is obtained by plotting the MCD signal

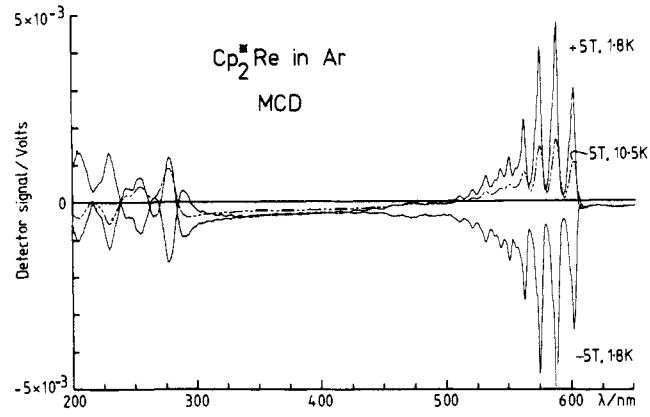

Figure 9. Magnetic circular dichroism of Cp^*_2Re in argon matrix at 1.8 K, recorded at +5 and -5 T magnetic flux density (solid line), and at 10.5 K, recorded at +5 T magnetic flux density (dotted line) (slit width 1 nm, scan speed 0.4 nm s^{-1}, 20 min deposition, sample temperature 313 K, deposition temperature 11 K).

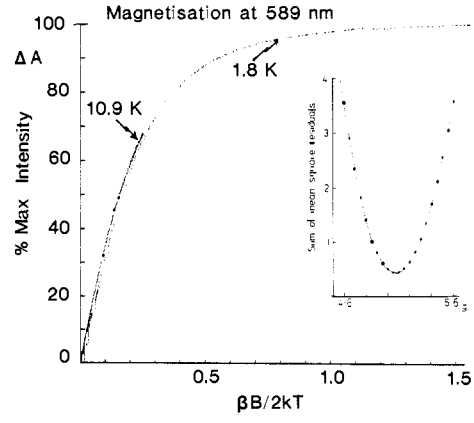

Figure 10. Magnetization curves obtained by recording circular dichroism at 589 nm and either 10.9 or 1.8 K as a function of magnetic flux density. Each dot represents an experimental point. The inset shows how the sum of the mean-square residuals varies with $g_\parallel$, when 30 representative points from the data are fitted to the expression in the text.

at a fixed wavelength against $\mu_B B/2kT$ as the magnetic field is increased (μ_B is the Bohr magneton, k the Boltzmann constant). The temperature, although nominally fixed, is measured at each point. The curve was recorded with the dichrograph on the λ = 589 nm maximum at two temperatures, 10.9 and 1.8 K over a field range 0-8 T. The curves obtained were essentially superimposable (Figure 10). When the field was reversed, almost perfect mirror images were obtained. The curve obtained at 1.8 K shows very strikingly the saturation which sets in when the Zeeman splitting exceeds kT. The signal appears to be wholly derived from the temperature-dependent C term; there is no contribution from a temperature independent B term. According to Schatz et al.[33]

$$\Delta A = K \int_0^1 n \tanh (n g_\parallel \mu_B B/2kT)\, dn$$

for a set of randomly oriented axial molecules with $g_\perp$ = 0 where

(32) Graham, R. G.; Grinter, R.; Perutz, R. N. *J. Am. Chem. Soc.*, in press.

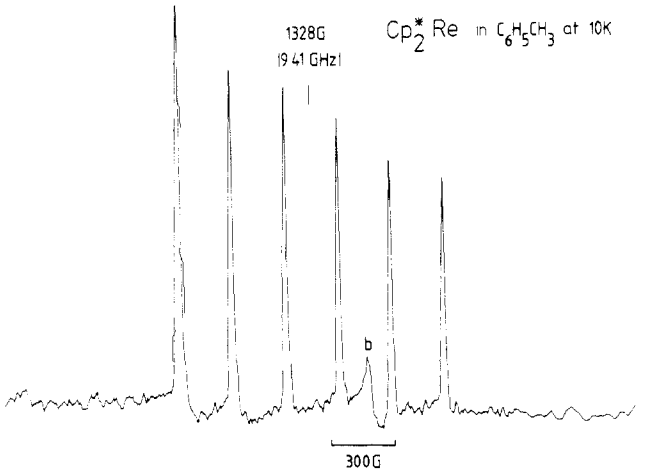

Figure 11. Electron spin resonance spectrum of a frozen toluene solution of Cp^*_2Re at 10 K recorded at 9.41 GHz. The major sextet is due to the $g_\parallel$ resonance coupled to ^{185}Re and ^{187}Re ($I = 5/2$). The feature b is an impurity in the cavity.

$n = \cos\theta$, θ is the angle between the molecular axis and the magnetic field, and K is a constant. A series of 30 representative points were fitted to this equation by adjusting K in a standard least-squares procedure for a series of values of $g_\parallel$. A plot of the mean-squared residuals per point against $g_\parallel$ yielded a well-defined minimum with $g_\parallel = 5.07 \pm 0.19$ (Figure 10, inset). (The error is not derived statistically but is set by the points where the value of the mean-square residuals is twice its minimum.) The fit of observed to calculated points is so good that the deviation never exceeds 1%, and the rms deviation is 0.66% of the maximum MCD signal. It is perhaps not surprising that no improvement was registered when we attempted to include the effect of deviations of $g_\perp$ from zero into the model.

Comparative magnetization measurements on $(\eta$-toluene$)_2V$, a d^5 sandwich complex with a $^2A_1$ ground state, gave g values close to two as expected.[32] Our measurements on Cp^*_2Re left us in no doubt, therefore, that this molecule has the other low-spin ground state, $^2E_2$ ($E_{5/2}$ with spin-orbit coupling). Magnetization measurements on Cp_2Re using the same instrument yield $g_\parallel = 5.35 \pm 0.37$, as expected somewhat higher than Cp^*_2Re.[32]

Electron Spin Resonance. Initial measurements of the ESR spectrum of $Cp_2{}^*Re$ in frozen solutions proved that the molecule is ESR silent down to 77 K, as indeed is expected for a rapidly relaxing $^2E_2$ ground state. Armed with the measurement of $g_\parallel = 4.87$ obtained from the MCD magnetization curve, we attempted to measure the ESR spectra of $Cp_2{}^*Re$ in frozen cyclohexane and toluene at ca. 4 K. The cyclohexane sample still gave no signal, but to our delight, the toluene solution gave a sharp sextet (Figure 11) centered at very low field with the typical "absorption" shape of parallel bands. The g value of 5.081 ± 0.003 (to first order) fitted excellently with the MCD, the sextet structure was readily explained by the $I = {}^5/_2$ nuclear spins of the two rhenium isotopes, $^{185,187}Re$ ($A = 22.29$ (6) mT = 1585 (3) MHz to first order, fwhm = 1.5 mT). The sextet intensity was reduced considerably at 22 K, disappeared by 42 K, and reappeared on cooling. No corresponding $g_\perp$ signal could be detected up to the field limit of this instrument indicating $g_\perp < 0.85$. Measurements up to higher field at NRC, Ottawa confirmed $g_\parallel$ but still failed to find $g_\perp$ with a field limit of 1.9 T, implying $g_\perp < 0.34$.

Since the line separations of the parallel features of the ESR spectrum are very regular, it appears that no second-order corrections are necessary. This can be understood, since second-order corrections to the parallel line position are proportional to $nA_\perp{}^2/(4g_\parallel\mu_B B_\parallel)$.[34] We can calculate a limit to $A_\perp$ from the lack of second-order shifts of $A_\perp < 200$ MHz. However, this information is insufficient to calculate useful limiting orbital populations.

Table XI. Vertical Ionization Energies and Relative Band Intensities in the He I and He II Spectra of Cp^*_2Re

band	KE[a] (eV)	IE[a] (eV)	relative intensity[b] He I	He II	He II/He I ratio
A	15.42	5.79	1.00	1.00	1.00
B	14.97	6.25	0.95	0.77	0.81
C	14.47	6.75	0.40	0.61	1.49
D1	13.92	7.30			
D2	13.77	7.45			
D			2.87	1.94	0.68
D3	13.62	7.60			
D4	13.16	8.05			
E	12.36	8.86	2.40	1.86	0.78
F	11.51	9.71	1.36	0.14	0.10
G1	10.96	10.26			
G2	10.25	10.96			
G			13.90	5.81	0.42
G3	9.90	11.32			
H1	8.70	12.52			
H2	7.99	13.22			
H			82.3		
H3	7.34	13.88			
I	4.83	16.39	7.2		

[a] Kinetic and ionization energies are quoted ±0.1 eV. [b] All intensity data are given relative to band A.

The g values for Cp^*_2Re confirm that we are concerned with a $^2E_2$ ground state. The most thorough study of such systems has been carried out by Ammeter.[5,9] He expresses the equations for the g values as

$$g_\parallel = g_e + 4kV\cos\alpha \qquad g_\perp = (g_e - 2x)\sin\alpha$$

where k is an orbital reduction factor and V a vibronic quenching parameter approaching zero for large Jahn–Teller coupling. The angle α measures the deviation from fivefold symmetry via $\tan\alpha = \delta_0/\zeta$ (applicable only if there is no Jahn–Teller stabilization), δ_0 is the static splitting resulting from symmetry reduction, ζ the spin–orbit coupling constant, and x depends on $\zeta/\Delta E$ where ΔE is the average energy gap between the occupied d orbitals and the $e_1(\pi)$ levels. If we assume $x \simeq 0.05$, then we derive $\tan\alpha < 0.81$ and $0.718 < kV < 0.728$. As pointed out by Ammeter,[5,9] the ligand carries orbital angular momentum of the same sign as the metal, so k remains high. Since ζ is much greater for Re than for the first-row metals, $\tan\alpha$ is considerably lower for Cp^*_2Re than for Cp^*_2Mn, but kV is increased (for Cp^*_2Mn in toluene glass with $x = 0.01$, $\tan\alpha = 1.60$, $kV = 0.595$).

Gas-Phase Photoelectron (PE) Spectra. He I and He II PE spectra of Cp^*_2Re are presented in Figure 12. The raw data are represented by points, while the solid lines show the result of convoluting the data with a nine point quartic least squares smoothing function. The band labeled He^+ in the He I spectrum is due to ionization of He atoms by He II radiation. Table XI gives the vertical IEs and the relative intensities of the peaks in the He I and He II spectra. Band intensities were determined from the areas of Gaussian/Lorentzian curves fitted to the spectra, and the bands normalized to an area for A of 1.0 in both He I and He II spectra.

The peaks of IE > 10 eV are assigned below mainly by analogy with PES of other decamethylmetallocenes[35] (see Table XII for assignment). The assignment of the crucial low-energy peaks is given in the Discussion after presenting the results of ligand field calculations. Assignments are given in terms of the full D_{5h} symmetry established.

Bands D and E, although doubtless containing some intensity due to ionization of metal d electrons, can be assigned to ionization of the predominantly ligand (π) e_1' (band D) and e_1'' (band E) orbitals. That peak E has a higher He II/He I intensity ratio

(33) Schatz, P. N.; Mowery, R. L.; Krausz, E. R. *Mol. Phys.* **1978**, *35*, 1537.
(34) Morton, J. R.; Preston, K. F. *J. Magn. Reson.* **1978**, *30*, 577.
(35) Cauletti, C.; Green, J. C.; Kelly, M. R.; Powell, P.; Van Tilborg, J.; Robbins, J.; Smart, J. *J. Electron Spectrosc. Relat. Phenom.* **1980**, *19*, 327.

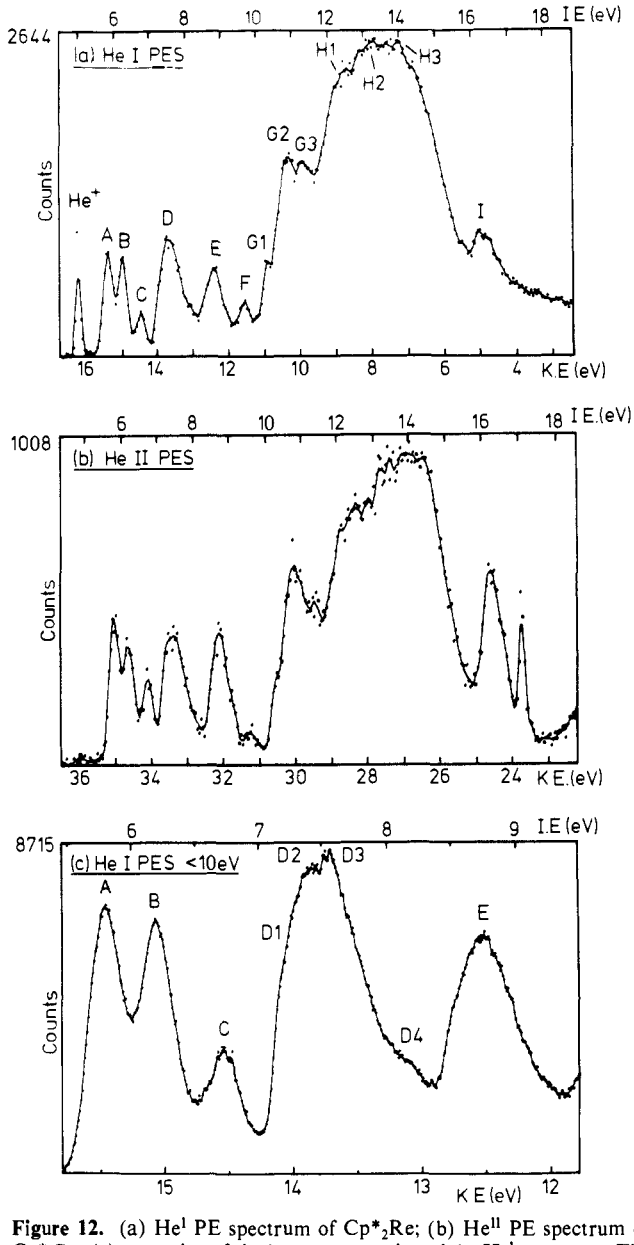

Figure 12. (a) He^{I} PE spectrum of Cp^*_2Re; (b) He^{II} PE spectrum of Cp^*_2Re; (c) expansion of the low-energy region of the He^{I} spectrum. The band labels refer to the text and Tables IX and X. The band marked He^+ is the self-ionization of He gas.

is indicative of this assignment, since the e_1'' orbitals have substantial metal d character and form the major portion of the M–C bonding, whereas the e_1' orbitals can have no d character by symmetry. Also the IEs of these peaks are similar to those found for the same orbitals in other Cp^*_2M and Cp_2M species.[35] However, e_1' ionization usually gives rise to a PE band with a sharper low IE edge than observed for band D, and in, for example, the spectrum of Cp_2Os,[36] the relative intensity changes between the $e_1'^{-1}$ and $e_1''^{-1}$ band in the He I and He II spectra are more dramatic than those observed for bands D and E. These differences may well be due to metal band ionizations underlying the main e_1' peak of band D (vide supra).

Band F, which has a very low He II/He I intensity ratio, much lower than any other band in the spectrum, is most likely due to a shake-up state associated with the E band ionizations. A likely candidate for the shake-up process is a_1' or $e_2' \rightarrow e_1''^*$, i.e., σ or $\delta \rightarrow \pi$ in $C_{\infty v}$ symmetry.

The PE spectra of Cp_2Co and Cp_2Ni also show peaks in this IE region which virtually disappear in their He II spectra; these may be due to similar processes.[35] The shoulder at IE 8.05 eV on band D could be due to the same shake-up transition accompanying e_1' ionization although another possibility here is the $^1\Sigma^+$ ($L = 0$) state which is predicted by the LF calculations to occur at 2.00 eV above the ion ground state (see Discussion).

Peaks G which appear as a prominent shoulder on the low IE side of band H are assigned as ionization of electrons localized on the methyl groups of the Cp* ligands; such shoulders do not occur in the spectra of Cp_2M compounds but are visible in all Cp^*_2M spectra.[35] Bands H are then assigned to C–H and C–C σ skeletal electrons, along with the a_1' and a_2'' ring π orbitals, while band I originates from deeper lying ligand σ orbitals having substantial C 2s character.

Ligand Field Calculations. As Cp^*_2Re is an open-shell molecule with a large spin-orbit coupling constant (ζ), numerous low-energy ion states are accessible by ionization of Re d electrons. Since the matrix experiments do not establish the energy separation of the $A_{1/2}$ state from $E_{5/2}$ ground state, ligand field calculations were performed on the d^4 configuration of $Cp^*_2Re^+$, including configuration interaction between all spin-orbit states involving occupancy of the $e_2'(\delta)$ and $a_1'(\sigma)$ metal orbitals. States involving $e_1''(\pi)$ occupancy were considered too high in energy to contribute significantly (Δ_1 too large). The CI matrices are given in Table XIII, and Table XIV shows the first-order ion-state energies (in

Table XII. Proposed Assignments of the Photoelectron Spectra of $Cp_2{}^*Re$

band	IE (eV)	assignment: (initial state)
A	5.79	$^3\Delta$ ($\Omega = 3$) + $^3\Delta$ ($\Omega = 2$): ($E_{5/2}' + A_{1/2}'$)
B	6.25	$^3\Sigma^-$ ($\Omega = 0$): ($E_{5/2}' + A_{1/2}'$) + $^3\Delta$ ($\Omega = 1$): ($A_{1/2}'$)
C	6.75	$^1\Delta$ ($\Omega = 2$) + $^1\Sigma^+$ ($\Omega = 0$): ($E_{5/2}' + A_{1/2}'$) + $^3\Sigma^-$ ($\Omega = 1$): ($E_{5/2}'$) + $^1\Gamma$ ($\Omega = 4$): ($E_{5/2}'$)
D	7.60	e_1' cp π orbitals + $^1\Sigma^+$ ($\Omega = 0$): ($E_{5/2}' + A_{1/2}'$)
E	8.86	e_1'' cp π and M–C bonding orbitals
F	9.71	a_1' or $e_2' \rightarrow e_1''^*$ shake-up associated with band E
G	10.96	methyl group electrons
H	13.22	C–C and C–H σ skeletal bonding orbitals + the a_1' and a_2'' ring π orbitals
I	16.39	lower energy C–C and C–H σ electrons

$C_{\infty v}$	D_{5h}	$C_{\infty v}$	D_{5h}
Correlations between $C_{\infty v}$ and D_{5h} Symmetry Representations[2]			
Σ^+	A_1'	Φ	E_2'
Σ^-	A_2'	Γ	E_1''
Π	E_1''	H	$A_1' + A_2'$
Δ	E_2'	Θ	E_1''

Table XIII. Configuration Interaction Matrices

$\Omega = 0$	$^1\Sigma^+$	$^3\Sigma^-$	$^1\Sigma^+$
$^1\Sigma^+$	$-16B + 9C + 2\Delta_2$	-2ζ	$2^{1/2}(4B + C)$
$^3\Sigma^-$	-2ζ	$-16B + 5C + 2\Delta_2$	0
$^1\Sigma^+$	$2^{1/2}(4B + C)$	0	$24B + 8C$

$\Omega = 2$	$^3\Delta$	$^1\Delta$
$^3\Delta$	$-8B + 5C + \Delta_2$	ζ
$^1\Delta$	ζ	$7C + \Delta_2$

Table XIV. Calculated First-Order Ion State Energies and Photoelectron Intensities for Cp^*_2Re[a]

ion state	energy (eV)	intensity ($E_{5/2}$)	intensity ($A_{1/2}$)
$^3\Delta$ ($\Omega = 3$)	$-8B + 5C + \Delta_2 - \zeta$	σ_a	σ_e
$^3\Delta$ ($\Omega = 2$)	$-8B + 5C + \Delta_2$	$0.5\sigma_a$	σ_e
$^3\Delta$ ($\Omega = 1$	$-8B + 5C + \Delta_2 + \zeta$	0	σ_e
$^1\Delta$ ($\Omega = 2$)	$7C + \Delta_2$	$0.5\sigma_a$	σ_e
$^1\Sigma^+$ ($\Omega = 0$)	$-16B + 9C + 2\Delta_2$	$0.5\sigma_e$	0
$^3\Sigma^-$ ($\Omega = 1$)	$-16B + 5C + 2\Delta_2$	σ_e	0
$^3\Sigma^-$ ($\Omega = 0$)	$-16B + 5C + 2\Delta_2$	$0.5\sigma_e$	0
$^1\Gamma$ ($\Omega = 4$)	$-16B + 7C + 2\Delta_2$	σ_e	0
$^1\Sigma^+$ ($\Omega = 0$)	$24B + 8C$	0	σ_a

[a] ζ = spin orbit coupling parameter; B and C = Racah electron repulsion parameters; Ω = total angular momentum of state; σ_e = photoionization cross section of metal e_2 orbital; σ_a = photoionization cross section of metal a_1 orbital.

(36) Cooper, G.; Green, J. C., unpublished work.

Table XV. Calculated Ion State Energies and Photoelectron Intensities for Cp^*_2Re Including Configuration Interaction

ion state	energy above ion ground state (eV)	intensity ($E_{5/2}$)	intensity ($A_{1/2}$)
$^3\Delta$ (Ω = 3)	0	σ_a	σ_e
$^3\Delta$ (Ω = 2)	0.16	$0.77\sigma_a$	$0.77\sigma_e$
$^3\Delta$ (Ω = 1)	0.45	0	σ_e
$^1\Delta$ (Ω = 2)	0.99	$0.23\sigma_a$	$0.23\sigma_e$
$^1\Sigma^+$ (Ω = 0)	2.00	$0.1\sigma_e$	$0.232\sigma_a$
$^3\Sigma^-$ (Ω = 1)	0.925	σ_e	0
$^3\Sigma^-$ (Ω = 0)	0.56	$0.785\sigma_e$	$0.2\sigma_a$
$^1\Gamma$ (Ω = 4)	1.225	σ_e	0
$^1\Sigma^+$ (Ω = 0)	1.054	$0.11\sigma_e$	$0.564\sigma_a$

Table XVI. Final Calculated Ligand Field Parameter Values

B = 0.05 eV	ζ = 0.225 eV
C = 0.15 eV	Δ_2 = 1.1 eV

terms of the parameters Δ_2, ζ, B, and C) and predicted PE band intensities for both the $E_{5/2}'$ and $A_{1/2}'$ states of neutral Cp^*_2Re, i.e., before diagonalization of the CI matrices.

Initial trial values for the Racah electron repulsion parameters B and C, and for Δ_2 and ζ, were obtained by consideration of their values in the closely related compounds Cp_2W[37] (d^4 configuration, ζ = 0.186) and Cp_2Os^+[36] (d^5 configuration, ζ = 0.31 eV), plus tabulated values for Re(I)[38] (d^7 configurations, B = 0.105, C = 0.146, ζ = 0.283 eV). Calculation of the ion-state energies and PE relative intensities (for both possible low-spin ground states of neutral Cp^*_2Re) was then carried out repeatedly, changing the parameters slightly each time, until a best fit of the energies and intensities to the experimental PES data was obtained. The energies were used as the most important criterion for assessing how good the fit was, the intensities being used in a secondary capacity to compare the predicted spectra with experiment after the ion-states energies had achieved reasonable agreement with the observed IEs. During this process the parameters were varied within the following ranges: $0.04 < B < 0.1$, $0.07 < C < 0.25$, $0.2 < \zeta < 0.3$, and $0.9 < \Delta_2 < 1.2$ eV. The eigenvalues of the CI matrices give the ion-state energies, while the eigenvectors are used for the band intensity calculations. The formulas used in these calculations were derived by using the following fractional parentage approach:[39] If the wave functions of the ion states subject to CI are given by the linear combinations (here the wavefunctions are denoted by the irreducible representations in the related $C_{\infty v}$ symmetry, see Table XII)

$$\Omega = 0: \quad |\psi\rangle = C_1|^1\Sigma^+\rangle + C_2|^3\Sigma^-\rangle + C_3|^1\Sigma^+\rangle$$

$$\Omega = 2: \quad |\psi\rangle = C_1'|^1\Delta\rangle + C_2'|^3\Delta\rangle$$

where the C's are the linear combination coefficients, then their photoelectron intensities are

For an $E_{5/2}'$ initial state:

$$\Omega = 0: \quad \sigma = (C_1/(2)^{1/2} + C_2/(2)^{1/2})^2\sigma_e$$

$$\Omega = 2: \quad \sigma = (-C_1'/(2)^{1/2} + C_2'/(2)^{1/2})^2\sigma_a$$

For an $A_{1/2}'$ initial state:

$$\Omega = 0: \quad \sigma = C_3^2\sigma_a$$

$$\Omega = 2: \quad \sigma = (C_1' + C_2')^2\sigma_e$$

It is the constants C which are obtained from the eigenvectors of the interaction matrices.

(37) Cox, P. A.; Grebenik, P.; Perutz, R. N.; Robinson, M. D.; Grinter, R.; Stern, D. R. *Inorg. Chem.* **1983**, *22*, 3614.
(38) Griffith, J. S. *The Theory of Transition Metal Ions*; Cambridge University Press: 1964.
(39) Cox, P. A. *Struct. Bonding (Berlin)* **1975**, *24*, 59.

Table XVII. Solid-State Magnetic Susceptibility Data on Cp^*_2Re

temp range (K)	field (T)	μ_{eff} (μ_B)	θ (K)
5–45	0.1	1.74 ± 0.02	−2.1 ± 0.5
5.5–45	0.5	1.61 ± 0.01	−0.44 ± 0.2
5.5–45	1.0	1.59 ± 0.01	−0.27 ± 0.14
5–45	2.0	1.59 ± 0.01	−0.57 ± 0.1
5–45	4.0	1.61 ± 0.01	−1.2 ± 0.1
5–45	0.5	1.66 ± 0.01	−0.46 ± 0.1
5–40	4.0	1.66 ± 0.01	−1.3 ± 0.2
101–283	1.0	1.71 ± 0.01	−13.1 ± 1.1
100–302	2.0	1.70 ± 0.01	−15.1 ± 1.0
98.5–300	4.0	1.69 ± 0.01	−12.0 ± 1.0
100–300	4.0	1.69 ± 0.01	−5.5 ± 0.7

The final calculated ion-state energies and corresponding PE band intensities are presented in Table XV, and the values of the parameters in Table XVI.

Solid-State Magnetic Susceptibility Measurements. The susceptibility data at low field: 0.1 and 0.5 do not fall on the same line (in a $1/\chi$ versus T plot) as the 1.0, 2.0, and 4.0 T runs. One possible explanation for these results is that there is a small ferromagnetic impurity which is important only at high temperatures (where the susceptibility from the Cp^*_2Re is small) and is completely saturated by 1.0 T. At low temperatures (<40 K) the susceptibilities coincide.

There are two regions of linear behavior in the $1/\chi$ versus T plots. For fields of 1.0 T and above, $T \geq 100$ K, μ_{eff} = 1.70 ± 0.02 with θ = −12.0 ± 5 K. For temperatures below 45 K μ_{eff} = 1.63 ± 0.03 with θ = −1 ± 1 K, with the equation $\chi = c/(T - \theta)$. Table XVII summarizes the results.

Solution Magnetic Measurements. The magnetic moment in *solution* at 298 K is found to be 1.95 ± 0.10, as determined by Evans' method,[19] somewhat larger than that found in the solid state (see Discussion).

Discussion

Synthesis. The unsubstituted rhenocene hydride, Cp_2ReH, is well known[40] and may be readily prepared by conventional methods. It has been shown to undergo simple Re–H bond cleavage upon low-temperature photolysis to yield the metallocene Cp_2Re, extensively characterized by matrix isolation spectroscopy.[11] Cp_2Re is unstable above about 20 K; recently the metal–metal bonded dimer $(Cp_2Re)_2$ has been synthesized by electron transfer from $Cp_2Re^-Li^+$,[41] and this is presumably the fate of matrix isolated monomeric Cp_2Re on matrix warmup. The permethylated precursor Cp^*_2ReH has not, to date, been prepared by conventional methods; recently we described the synthesis of $Cp^*_2WH_2$ with tungsten atoms,[42] and the preparation of Cp^*_2ReH from rhenium atoms is a further example of this route to decamethylmetallocene hydrides which are presently inaccessible via classical methods.

The photolytic conversion of Cp^*_2ReH into Cp^*_2Re presumably proceeds via simple homolysis of the Re–H bond to produce H$^\bullet$, although attempts to detect the latter by low-temperature (77 K) photolysis in the cavity of an ESR spectrometer were unsuccessful. The kinetic stability of Cp^*_2Re, as compared with the unsubstituted analogue, is a dramatic indication of the effect of permethylating the cyclopentadienyl rings; the latter achieves steric saturation and prevents dimerization of the 17-electron metallocene to form an 18-electron metal–metal bonded species analogous to $(Cp_2Re)_2$ (vide supra). Permethylation also affects the electronic structure to a limited extent, as is demonstrated by the spectroscopic studies discussed below.

Spectra and Structure in Low-Temperature Matrices and Glasses. *The matrix MCD spectra and the ESR spectra* in frozen toluene establish beyond doubt that the ground state of *molecular* Cp^*_2Re is $^2E_2$ ($E_{5/2}$ with spin-orbit coupling). The high values

(40) Green, M. L. H.; Pratt, L.; Wilkinson, G. *J. Chem. Soc.* **1958**, 3916.
(41) Pasman, P.; Snel, J. J. M. *J. Organomet. Chem.* **1984**, *276*, 387.
(42) Cloke, F. G. N.; Green, J. C.; Green, M. L. H.; Morley, C. P. *J. Chem. Soc., Chem. Commun.* **1985**, 945.

Table XVIII. Skeletal Modes of Decamethylmetallocenes and Rhenocene ($\bar{\nu}$/cm^{-1})

	Cp^*_2Fe[a] solid ground state	$[Cp^*_2Fe^+](PF_6^-)$[a] solid ground state	$^2E_{1u}$ excited state	Cp^*_2Re Ar matrix ground state	$E_{3/2}$ excited state	Cp^*_2Re solid ground state	Cp_2Re[b] N_2 matrix ground state
ν_s (a_1)	169	173				160	326
sym tilt (e_1)	378	369	370	383.3[c-e]	390.6[c,e]	378	
				384	393		
ν_a (a_2)	455	454		313			316
asym tilt (e_1)	515	536		350/367			298
⊥ ring def	595	595		586		587	

[a] Reference 7. [b] Reference 11. [c] The upper figure is the average from the vibrational progression; the lower figure is the (0,0) to (0,1)/(1,0) interval. [d] The anharmonicity constant for this mode, $\omega_e x_e = 0.28$ (7) cm^{-1}, giving $\omega_e = 384.6$ (4) cm^{-1}. [e] An alternative assignment for these bands is to an a_{1g} mode formed by coupling of ν_5 (a_{1g}) to the symmetric ring carbon–methyl deformation δ_s (C–CH_3) (see text).

of $g_\parallel$ for both Cp^*_2Re and Cp_2Re indicate that there is surprisingly little quenching of orbital angular momentum by delocalization onto the ligands. As expected, delocalization is greater for the substituted metallocene. The values of the hyperfine coupling are also consistent with this ground state.

MCD spectroscopy has proved particularly useful to us for establishing the paramagnetism of unstable metallocenes with two unpaired electrons or with high orbital angular momentum. Determination of g values has, until recently, been achieved by comparison of band areas for absorption and MCD. We have now refined the newer method of determining the magnetization curve by measurements at lower temperature and higher magnetic field and by very accurate measurement of these two parameters. It then became important to test the method on samples with known g values. The comparison of the ESR- and MCD-derived g values for Cp^*_2Re provided an ideal test for a very anisotropic system. The MCD magnetization curve allowed an excellent determination of $g_\parallel$, but it did not prove sensitive to small deviations of $g_\perp$ from zero.

Ammeter has demonstrated by ESR that first-row d^5 and d^7 metallocenes exhibit a dynamic Jahn–Teller (JT) distortion. He argues that the JT distortion energy never exceeds the energy of the JT active mode, at most 1350 cm^{-1}. We have shown previously that spin-orbit coupling is able to quench the JT distortion in third-row metallocenes.[37] For instance, in the case of Cp^*_2Re the spin-orbit energy 2ζ is ca. 4000 cm^{-1} (see below), whereas likely JT modes are still below 1400 cm^{-1}. Nevertheless, Cp^*_2Re cannot have perfect D_5 symmetry otherwise $g_\perp$ would be zero and the ESR spectrum would be unobservable.[9] Since the MCD and ESR spectra point to an $E_{5/2}$ ground state and there is no population of any other levels at low temperature, we can predict the magnetic moment for this two-level system with the Van Vlec equation[43]

$$\mu_\parallel^2 = 0.75 g_\parallel^2 = 17.79 \qquad \mu_\perp^2 = 0.75 g_\perp^2 \leq 0.2$$

$$\langle \mu \rangle = \left[\frac{1}{3}(\mu_\parallel^2 + 2\mu_\perp^2) \right]^{1/2} = 2.44\text{–}2.45\ \mu_B$$

The visible absorption and fluorescence spectra are probably the most highly resolved of any recorded for an organometallic. Such sharp spectra have been associated with high symmetry.[16] In the case of Cp^*_2Re we may surmise that the eclipsed structure is rigid at low temperatures because of steric hindrance, whereas the unsubstituted metallocenes such as Cp_2Re exhibit ring disorder. As a result the spectra of Cp^*_2Re are appreciably sharper than those of Cp_2Re. In the laser-induced fluorescence spectra bands are resolved to the base line, and the main bands have a full width at half maximum of only ca. 9 cm^{-1}. The visible absorption and emission bands of Cp_2Re, which have their (0,0) component at 20411 cm^{-1}, were assigned to a ligand-to-metal charge-transfer band ($e_1'^3\, a_1'^2\, e_2'^4 \leftarrow e_1'^4\, a_1'^2\, e_2^3$, $E_{3/2} \leftarrow E_{5/2}$). On methylation of the rings, the e_1' level is expected to rise in energy reducing the transition energy. In line with this argument, we observe the (0,0) transition of Cp^*_2Re at 16572 ± 2 cm^{-1} (compare also $Cp^*_2Fe^+$ and Cp_2Fe^+).[7] Such a rise in energy of the highest ring levels on methylation has been detected directly by photoelectron spectroscopy of sandwich complexes.[3,6,35] Our assignment is also consistent with the positive sign of the MCD signal, as we demonstrated for Cp_2Re.[11]

It is well established that energy transfer in matrices is rapid when the transfer is close to resonant even at extremes of dilution.[44] The observation that irradiation into the higher energy progression causes emission in the lower energy progression is entirely consistent with such energy transfer. The excess energy of ca. 140 cm^{-1} could be transferred readily to matrix phonons.

The fine structure on the major visible bands is observed only in absorption, not in emission. Moreover, the structure changes significantly on annealing (Figure 6). In N_2 matrices, it is particularly clear that annealing does not simply enhance the resolution. All these observations are consistent with the idea of coupling to matrix phonon modes in the excited state. However, it is surprising that the transition energy is as low as ca. 20 cm^{-1} compared with the expected 32 cm^{-1} for pure argon.[31] The separation appears to be smaller for Cp^*_2Re than for the metallocenes, Cp_2Re, Cp_2Mo, and Cp_2W (interval 20–60 cm^{-1}),[11,16] but this may be the result of better energy resolution at longer wavelength.

The vibrational fundamentals of matrix-isolated Cp^*_2Re in the ground and LMCT excited state may be obtained from LIF and visible absorption spectra in addition to the usual IR spectra. The ligand modes of the IR spectrum of matrix-isolated Cp^*_2Re are exceedingly similar to those observed in the spectrum of solid Cp^*_2Fe, whereas $Cp^*_2Fe^+$ salts exhibit appreciably different spectra. The similarity of the Cp^*_2Re and Cp^*_2Fe spectra speak strongly against any Jahn–Teller distortion. For comparison, Cp_2Cr and Cp_2Co show substantially different ligand modes from Cp_2Fe because of Jahn–Teller distortions.[16,45]

As expected, the skeletal modes of Cp^*_2Re are appreciably different from those of Cp^*_2Fe (Table XVIII). The IR band at 313 cm^{-1} is assigned to the antisymmetric ring–metal–ring stretch and is almost coincident with the corresponding band of Cp_2Re. Either the 350- or the 367-cm^{-1} band must be the antisymmetric ring tilting mode; this is substantially lower than for Cp^*_2Fe. Most interestingly, the progressions in the absorption and the LIF spectra of Cp^*_2Re occur at frequencies about 60 cm^{-1} higher than for Cp_2Re. A very similar effect has been observed[7] in the absorption spectra of $Cp^*_2Fe^+$ and Cp_2Fe^+. Both Duggan and Hendrickson and we assigned the progressions of the unsubstituted metallocenes to ν_4, the ring–metal–ring symmetric stretching mode.[7,11,16] Duggan and Hendrickson argue that the transition between $^2E_{2g}$ and $^2E_{1u}$ states of $Cp^*_2Fe^+$ is coupled to the e_{1g} symmetric tilting vibration. The same assignment could be applicable to Cp^*_2Re, but it is unclear to us why there is no excitation of the symmetric ring–metal–ring stretch in the decamethylmetallocenes. The latter vibration is found at 160 cm^{-1} in Raman spectra of solid Cp^*_2Re, in excellent agreement with the position for $Cp^*_2Fe^+$ (see Table XVIII).

An alternative interpretation, apparently not considered by the earlier authors, is that the totally symmetric deformation of the C–CH_3 bonds is coupled to the symmetric ring–metal–ring stretch resulting in A_1 modes at 384 and 160 cm^{-1}. The electronic transition would then be coupled to the upper member of this pair.

(43) Golding, R. M. *Applied Wave Mechanics*; Van Nostrand: New York, 1969; p 229.

(44) Dubost, H. *Springer Series in Chemical Physics* **1984**, *34*, 146. Bondybey, V. E. *Ann. Rev. Phys. Chem.* **1984**, *35*, 591.

(45) Grebenik, P. D. Phil. Thesis, University of Oxford, 1981.

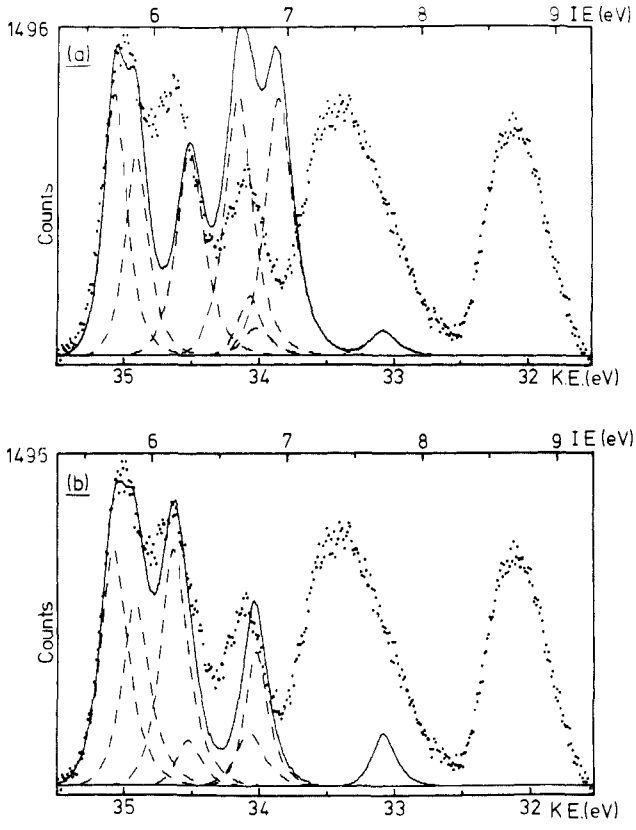

Figure 13. Fit of calculated to observed PE spectrum in the region <10 eV IE: (a) for the $E_{5/2}$ ground state of Cp^*_2Re and (b) for the $A_{1/2}$ ground state.

Comparison of the LIF and visible absorption spectra shows that there is a small but significant *increase* of 7 cm^{-1} in the coupled mode in the excited state. The LIF and absorption spectra also show very weak coupling to ligand modes notably at 1033 cm^{-1} (LIF) and 1024 cm^{-1} (absorption).

Electronic Structure and Photoelectron Spectra in the Gas Phase. While the spectra in low-temperature matrices establish beyond doubt that the ground state of Cp^*_2Re is $E_{5/2}$, they do not pinpoint other low-lying electronic states. The best source of this information is the photoelectron spectrum in the region below 10 eV. We now use the results of the ligand field calculations to assign the spectrum.

Figure 13 shows curve fits of the calculated PE band energies and intensities originating from Re d orbital ionization to the He II experimental data (at <10 eV IE) assuming $E_{5/2}'$ and $A_{1/2}'$ neutral molecule ground states, respectively. Fits were also applied to the He I spectrum, but they were worse than those obtained to the He II spectrum in both cases, primarily due to the lower relative intensity of band C. The He II spectrum can be expected to give more reliable comparisons with the LF calculations, since peak intensities are not influenced by near threshold effects which are possible at the He I energy of 21.2 eV. In all cases the fits were normalized to the experimental data by obtaining a best fit of A. By analogy with the PE spectra particularly of Cp_2Os[36] but also of other metallocenes,[35,46] the photoionization cross section of the e_2' orbitals was assumed to be (a) 1.2 × the cross section of the a_1' orbital in the fits to the He II data and (b) 1.4 × the a_1' cross section in fitting the He I data. This was taken into account in the fits by setting the bands originating from e_2' ionization to be (a) 1.2 × wider than those due to a_1' ionization and (b) 1.2 × wider and 1.17 × higher than the a_1' peaks.

As can be seen from Figure 13, for neither possible low-spin molecular ground state is the fit of the predicted spectrum to the experimental data satisfactory, although that obtained assuming the $A_{1/2}$ ground state is certainly the better of the two, mainly due to transitions to the $^3\Sigma^-$ ($\Omega = 1$) and $^1\Gamma$ ($\Omega = 4$) ion states being disallowed from this ground state (see Table XV). The spectrum would however be adequately described by a linear combination of the two calculated spectra, in the approximate ratio, $A_{1/2}$:$E_{5/2}$ = 0.8:0.2. One is therefore led to the conclusion that possibly the $E_{5/2}$ and the $A_{1/2}$ states are in thermal equilibrium at the PES data collection temperatures (360–375 K), with the $A_{1/2}$ state being marginally the more stable. If one accepts this, then the large He II/He I intensity ratio of band C, which is normally indicative of an $a_1'^{-1}$ band rather than an $e_2'^{-1}$ band, can be explained by intensity from the $A_{1/2} \rightarrow {}^1\Sigma^+$ transition at this energy. Also the larger ratio of band A than band B would be due to a larger proportion of a_1 ionization character originating from the $E_{5/2}' \rightarrow {}^3\Delta$ transition.

By using the ligand field parameters derived above for $Cp^*_2Re^+$ (Table XVI), the $A_{1/2}$ ($\Omega = 1/2$) neutral molecule state, which is favored by low B and high Δ_2 values, is calculated to be 0.125 eV above the $E_{5/2}$ ($\Omega = 5/2$) state. In the neutral molecule, however, electron repulsion should be relatively lower than in the positive ion due to greater orbital extension, and it is possible that metal–ligand interactions will be stronger due to better orbital overlap, leading to a higher Δ_2 value. $A_{1/2}$ therefore could be the ground state of Cp^*_2Re in the gas phase.

Electronic Structure in the Solid State and Solution. The value of μ_{eff} obtained from the solid state susceptibility measurements (Table VII) is much closer to that expected for the $A_{1/2}$ state (1.73 μ_B). We, therefore, conclude that $A_{1/2}$ is the ground state in the crystal over the temperature range investigated.

The experimental solution magnetic moment is, however, 1.95 μ_B at 298 K, suggesting both $E_{5/2}$ and $A_{1/2}$ states are occupied. However, variable temperature absorption spectra in solution give evidence that only one electronic state is occupied significantly up to 340 K and that this is the same state as in low-temperature matrices and frozen solution.

Conclusion

Cp^*_2Re has an eclipsed sandwich structure in the solid state; magnetic susceptibility measurements indicate an $A_{1/2}$ ground state in this phase. However, measurements of MCD spectra and ESR spectra show that the molecule adopts the $E_{5/2}$ ground state in Ar and N_2 matrices and in frozen toluene. The gas-phase photoelectron spectrum of Cp^*_2Re suggests an equilibrium between $A_{1/2}$ and $E_{5/2}$ states at higher temperatures. The solution magnetic moment is lower than expected for an $E_{5/2}$ state also suggesting an equilibrium. However, variable temperature absorption spectra in solution indicate occupation of the $E_{5/2}$ state only.

Acknowledgment. We are grateful to Professor R. E. Hester for use of the IR and Raman spectrometers and to SERC for financial support. We particularly acknowledge the assistance of Dr. A. J. Thomson and Dr. P. M. A. Gadsby (UEA) and Dr. J. R. Morton (NRC, Ottawa) in recording ESR spectra and Dr. N. Edelstein (L.B.L., Berkeley) for recording the solid state magnetic susceptibility. We are also indebted to H. C. Starck (Berlin) for a generous gift of rhenium metal.

Registry No. Cp^*_2ReH, 98814-96-1; Cp^*_2Re, 98814-97-2; Re, 7440-15-5.

Supplementary Material Available: Listings of mean planes and anisotropic thermal parameters (3 pages); listing of observed and calculated structure factors (9 pages). Ordering information is given on any current masthead page.

(46) Evans, S.; Green, M. L. H.; Jewitt, B.; King, G. H.; Orchard, A. F. *J. Chem. Soc., Faraday Trans. 2* **1974**, *70*, 356.